Prospects for Bc $\to \tau\nu$ ($\tau \to 3\pi\nu$) at FCC-ee

FCC Physics general meeting

May 31, 2021

Y. Amhis, **C. Helsens**, D. Hill, O. Sumensari

Prospects for $B_c^+ \to \tau^+ \nu_\tau$ at FCC-ee

Yasmine Amhis[1], Clément Helsens[2], Donal Hill[3], Olcyr Sumensari[1]

[1] *Université Paris-Saclay, CNRS/IN2P3, IJCLab, 91405 Orsay, France*
[2] *European Organization for Nuclear Research (CERN), Geneva, Switzerland*
[3] *Institute of Physics, École Polytechnique Fédérale de Lausanne (EPFL), Lausanne, Switzerland*

Email: **yasmine.amhis@ijclab.in2p3.fr, clement.helsens@cern.ch, donal.hill@cern.ch, olcyr.sumensari@ijclab.in2p3.fr**

https://arxiv.org/abs/2105.13330
To be submitted to JHEP

First FCC analysis to use common software tools from EDM4hep through to final analysis

Outline

- The measurement
- The context

The measurement

Abstract

This paper presents the prospects for a precise measurement of the branching fraction of the leptonic $B_c^+ \to \tau^+\nu_\tau$ decay at the Future Circular Collider (FCC-ee) running at the Z-pole. A detailed description of the simulation and analysis framework is provided. To select signal candidates, two Boosted Decision Tree algorithms are employed and optimised. The first stage suppresses inclusive $b\bar{b}$, $c\bar{c}$, and $q\bar{q}$ backgrounds using event-based topological information. A second stage utilises the properties of the hadronic $\tau^+ \to \pi^+\pi^+\pi^-\bar{\nu}_\tau$ decay to further suppress these backgrounds, and is also found to achieve high rejection for the $B^+ \to \tau^+\nu_\tau$ background. The number of $B_c^+ \to \tau^+\nu_\tau$ candidates is estimated for various Tera-Z scenarios, and the potential precision of signal yield and branching fraction measurements evaluated. The phenomenological impact of such measurements on various New Physics scenarios is also explored.

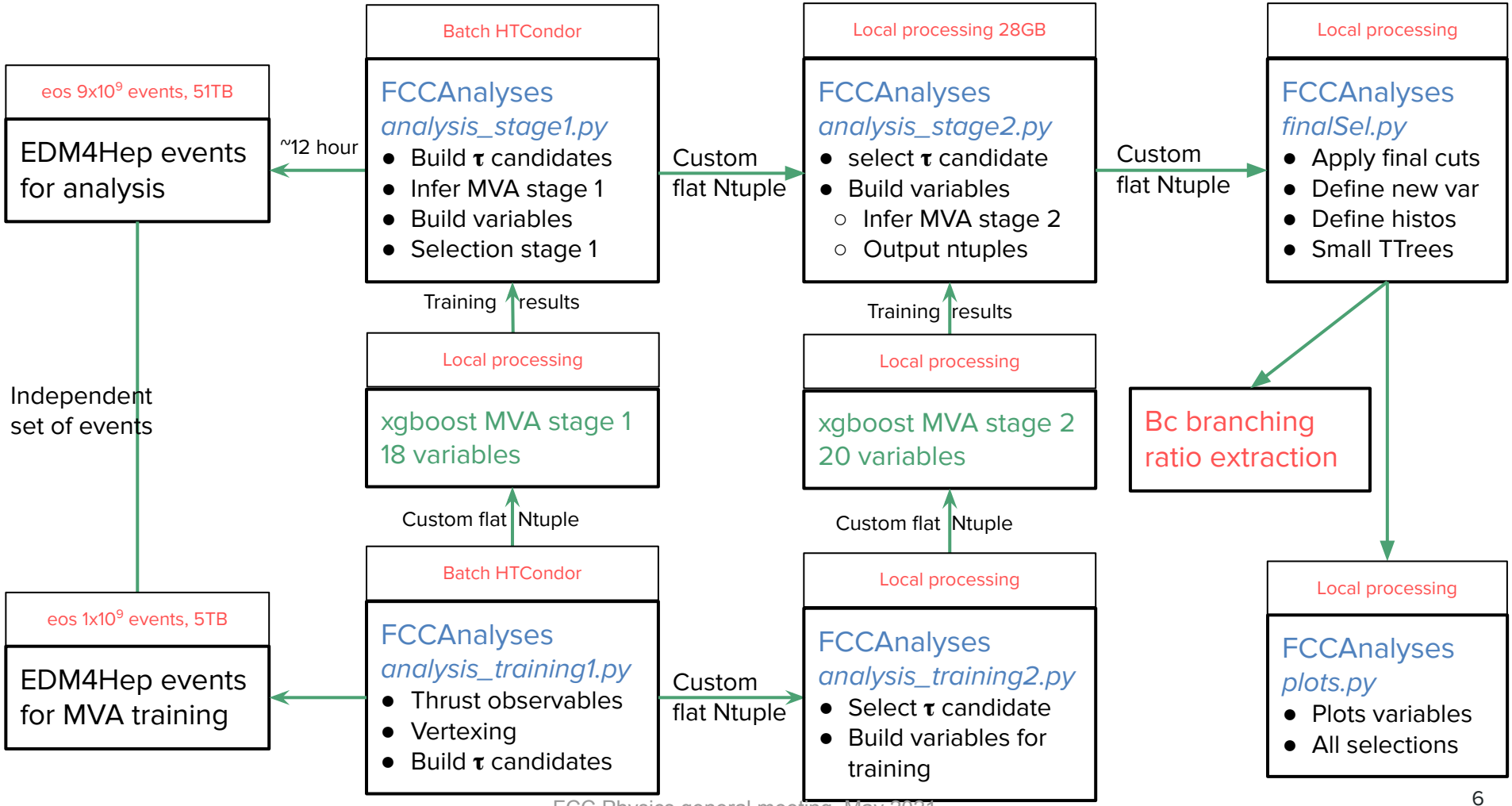
eos 9x10^9 events, 51TB
EDM4Hep events for analysis
~12 hour
Batch HTCondor
FCCAnalyses
analysis_stage1.py
Build τ candidates
Infer MVA stage 1
Build variables
Selection stage 1
Custom flat Ntuple
Local processing 28GB
FCCAnalyses
analysis_stage2.py
select τ candidate
Build variables
Infer MVA stage 2
Output ntuples
Custom flat Ntuple
Local processing
FCCAnalyses
finalSel.py
Apply final cuts
Define new var
Define histos
Small TTrees
Training results
Local processing
xgboost MVA stage 1
18 variables
Training results
Local processing
xgboost MVA stage 2
20 variables
Bc branching ratio extraction
Independent set of events
Custom flat Ntuple
Custom flat Ntuple
eos 1x10^9 events, 5TB
EDM4Hep events for MVA training
Batch HTCondor
FCCAnalyses
analysis_training1.py
Thrust observables
Vertexing
Build τ candidates
Custom flat Ntuple
Local processing
FCCAnalyses
analysis_training2.py
Select τ candidate
Build variables for training
Local processing
FCCAnalyses
plots.py
Plots variables
All selections

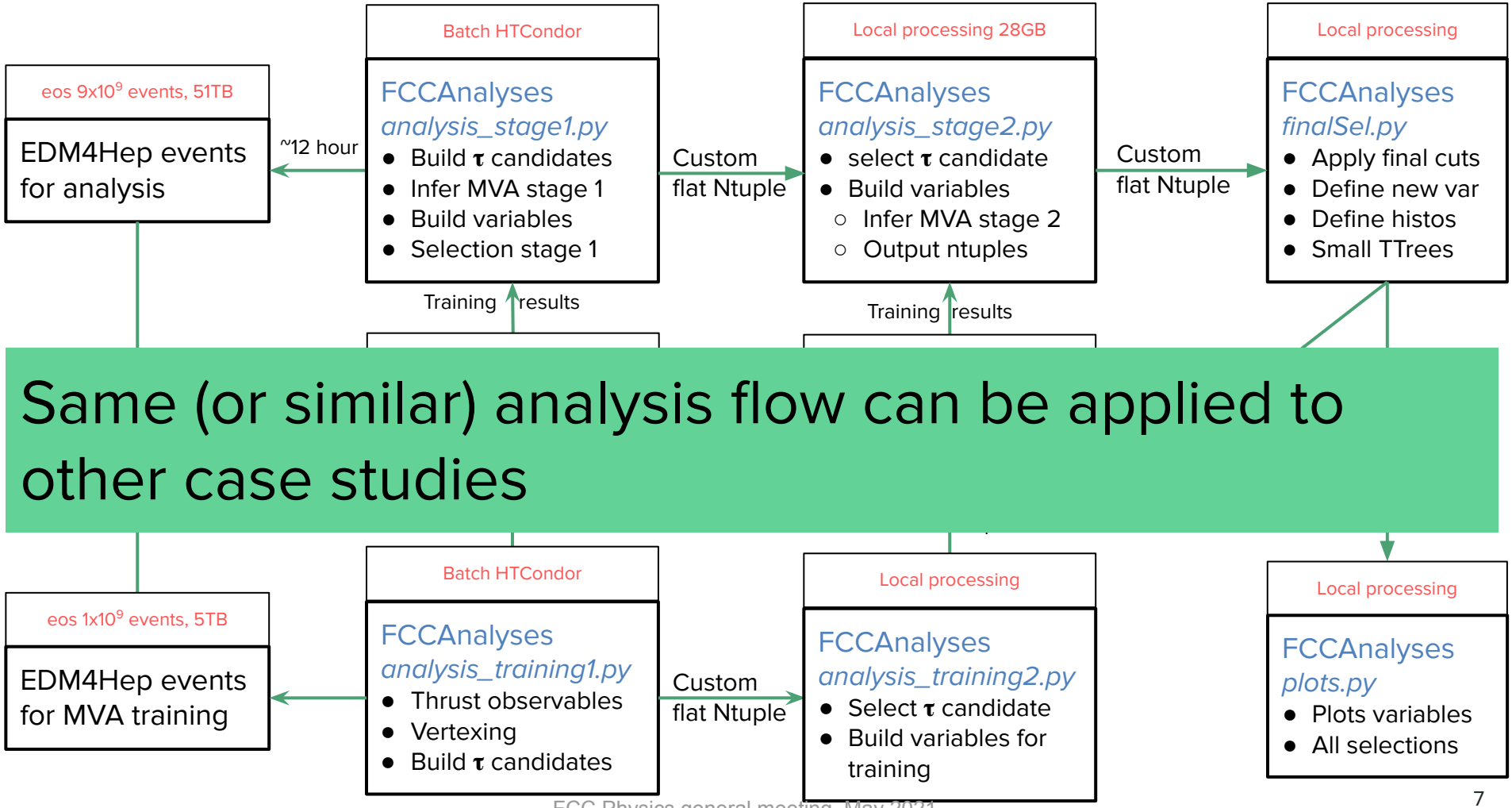
eos 9x10^9 events, 51TB
EDM4Hep events for analysis
~12 hour
Batch HTCondor
FCCAnalyses
analysis_stage1.py
Build τ candidates
Infer MVA stage 1
Build variables
Selection stage 1
Training results
Custom flat Ntuple
Local processing 28GB
FCCAnalyses
analysis_stage2.py
select τ candidate
Build variables
Infer MVA stage 2
Output ntuples
Training results
Custom flat Ntuple
Local processing
FCCAnalyses
finalSel.py
Apply final cuts
Define new var
Define histos
Small TTrees
Same (or similar) analysis flow can be applied to other case studies
eos 1x10^9 events, 5TB
EDM4Hep events for MVA training
Batch HTCondor
FCCAnalyses
analysis_training1.py
Thrust observables
Vertexing
Build τ candidates
Custom flat Ntuple
Local processing
FCCAnalyses
analysis_training2.py
Select τ candidate
Build variables for training
Local processing
FCCAnalyses
plots.py
Plots variables
All selections

First stage MVA variables

The BDT is trained using the following features:

- Total reconstructed energy in each hemisphere;
- Total charged and neutral reconstructed energies in each hemisphere;
- Charged and neutral particle multiplicities in each hemisphere;
- Number of tracks in the reconstructed PV;
- Number of reconstructed 3π candidates in the event;
- Number of reconstructed vertices in each hemisphere;
- Minimum, maximum, and average radial distance of all decay vertices from the PV.

First stage MVA

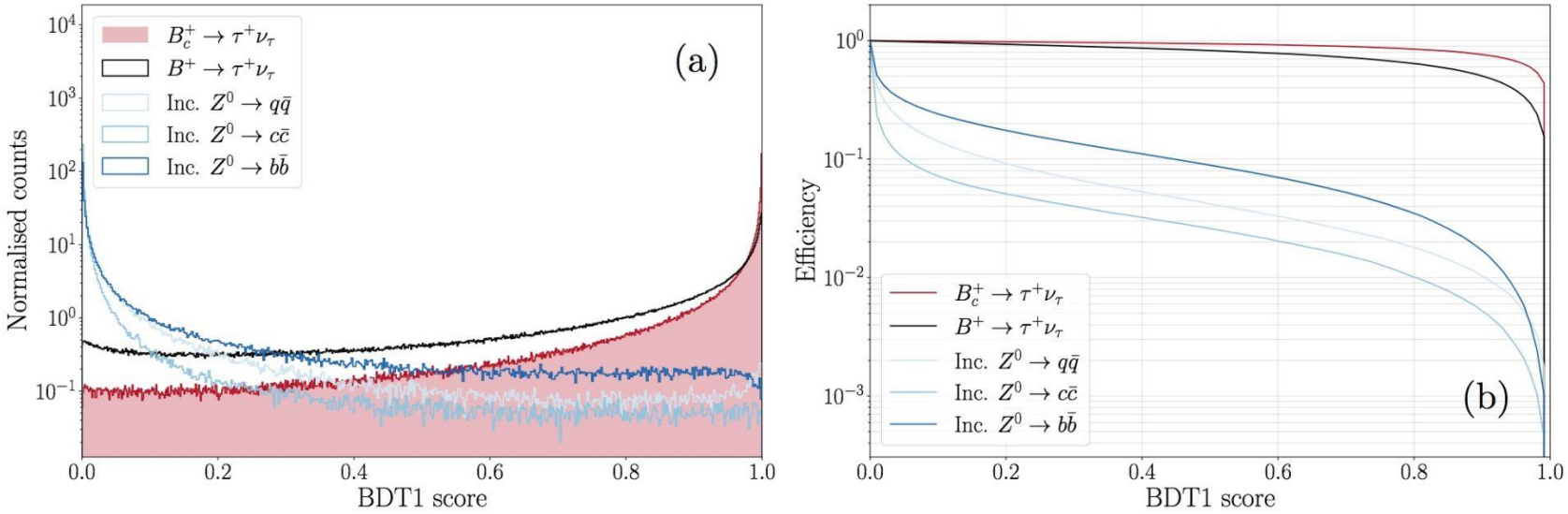

Figure 2: (a) First-stage BDT distribution in signal, $B^+ \to \tau^+\nu_\tau$ background, and inclusive Z background. (b) Efficiency of the first-stage BDT as a function of cut value.

Second stage MVA variables

The BDT is trained on the following features:

- 3π candidate mass, and masses of the two $\pi^+\pi^-$ combinations;
- Number of 3π candidates in the event;
- Radial distance of the 3π candidate from the PV;
- Vertex χ^2 of the 3π candidate;
- Momentum magnitude, momentum components, and impact parameter (transverse and longitudinal) of the 3π candidate;
- Angle between the 3π candidate and the thrust axis;
- Minimum, maximum, and average impact parameter (longitudinal and transverse) of all other reconstructed decay vertices in the event;
- Mass of the PV;
- Nominal B energy, defined as the Z mass minus all reconstructed energy apart from the 3π candidate.

Second stage MVA

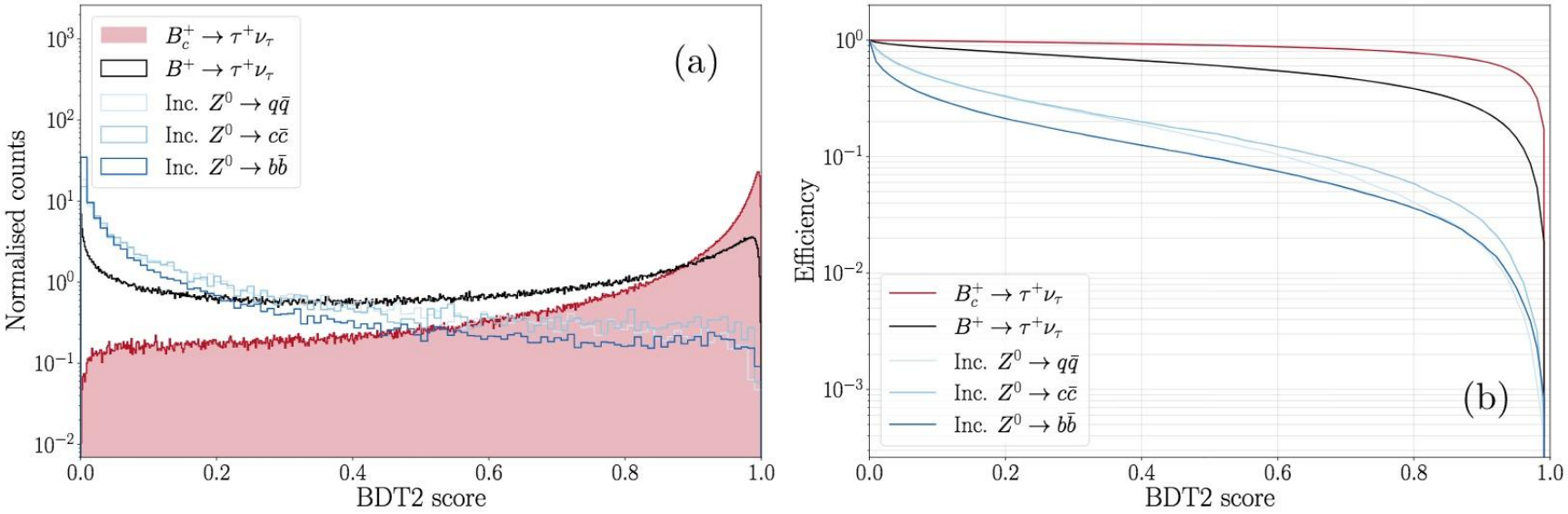

Figure 3: (Left) Second-stage BDT distribution in signal, $B^+ \to \tau^+\nu_\tau$ background, and inclusive Z background. (Right) Efficiency of the second-stage BDT as a function of cut value.

Background composition

Prior to the BDT cut optimisation, none of the 10^9 inclusive $Z \to c\bar{c}$ and $Z \to q\bar{q}$ events are found to pass sufficiently tight cuts on both BDTs. As such, background from these sources is not considered in the optimisation or subsequent fit studies. After the same cuts, the remaining statistics in the inclusive $Z \to b\bar{b}$ sample are found to be insufficient for determining the background rejection accurately in the cut optimisation. To boost the background statistics for the optimisation, samples of exclusive b-hadron decays are generated, where the decay modes are chosen based on the composition of the remaining inclusive $Z \to b\bar{b}$ sample. The following decays are considered:

- $B \to D\tau^+\nu_\tau$
- $B \to D^*\tau^+\nu_\tau$
- $B \to D\pi^+\pi^+\pi^-$
- $B \to D^*\pi^+\pi^+\pi^-$
- $B \to DD_s^+$
- $B \to D^*D_s^+$
- $B \to D^*D_s^{*+}$

where $B \in \{B^0, B^+, B_s^0, \Lambda_b^0\}$ and the corresponding $D \in \{D^-, \overline{D}^0, D_s^-, \Lambda_c^-\}$. In each of the exclusive b-hadron samples, all of the b-hadron decay products are decayed inclusively. The list of exclusive decays considered is not exhaustive, and covers around 10% of the decay width for each B hadron. As a result, a factor 2.5 difference in rate relative to the inclusive $Z \to b\bar{b}$ sample is observed after tight BDT cuts. This factor is used to scale the exclusive sample yield estimates in the optimisation procedure, in order to avoid underestimating the expected background level.

Background estimation

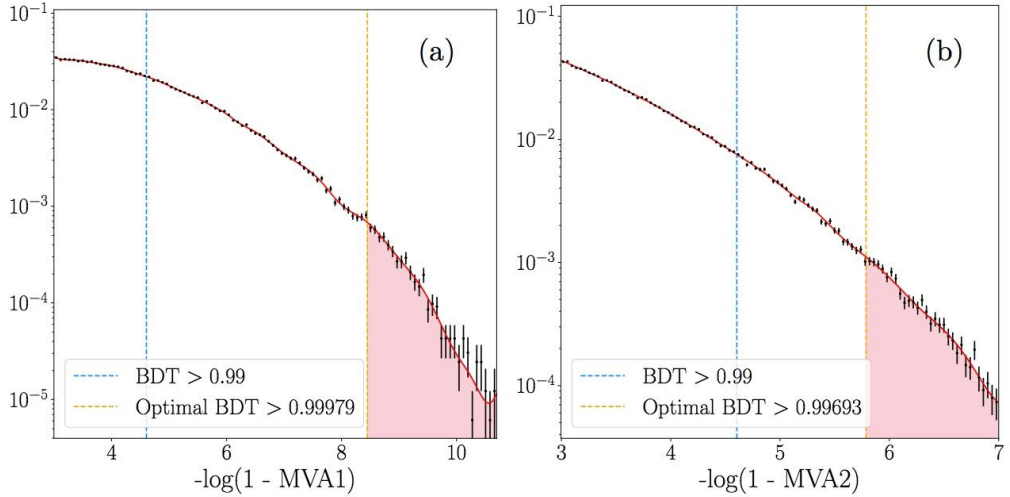

Figure 4: (a) BDT1 distribution above 0.95 for a combined sample of exclusive b-hadron decays. (b) BDT1 distribution above 0.95 for a combined sample of exclusive b-hadron decays. The cubic spline parameterisations are shown by solid red lines, example cuts of BDT > 0.99 by the dashed blue lines, and the optimal BDT cuts by the dashed orange lines. The background efficiency given prior cuts of > 0.95 on both BDTs is given by the product of the spline integrals above the optimal cuts (red areas), where each integral is normalised to the respective spline integral across the full range.

Discriminating variable

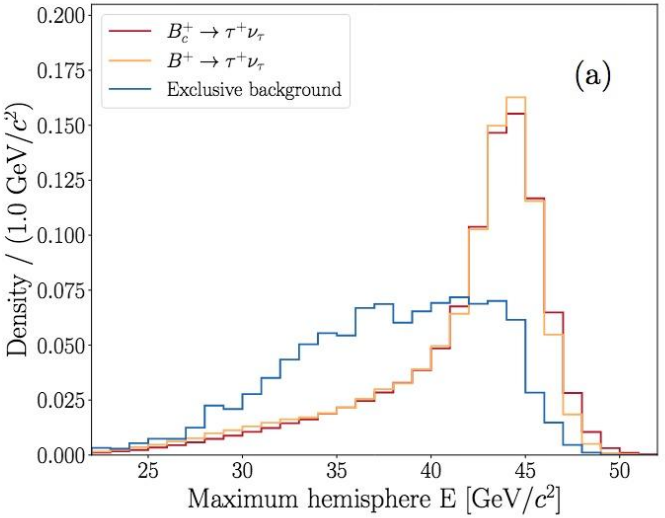

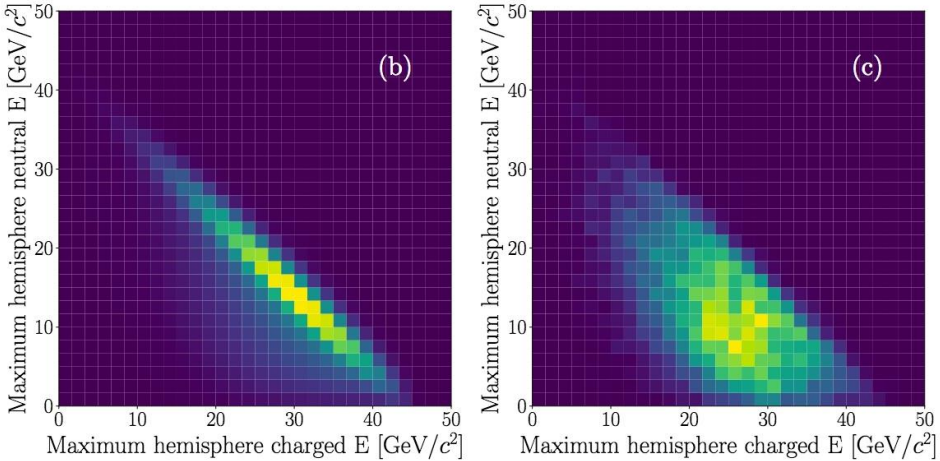

Figure 5: (a) Distribution of total hemisphere energy for the maximum energy hemisphere. Signal and $B^+ \to \tau^+\nu_\tau$ decays closely follow the expected distribution for an inclusive b-quark decay from a Z, whereas the background distribution is biased downwards by the selection. (b/c) Relationship between the total charged and neutral energy in the maximum energy hemisphere for $B_c^+ \to \tau^+\nu_\tau$/ inclusive $Z \to b\bar{b}$ events.

Fit

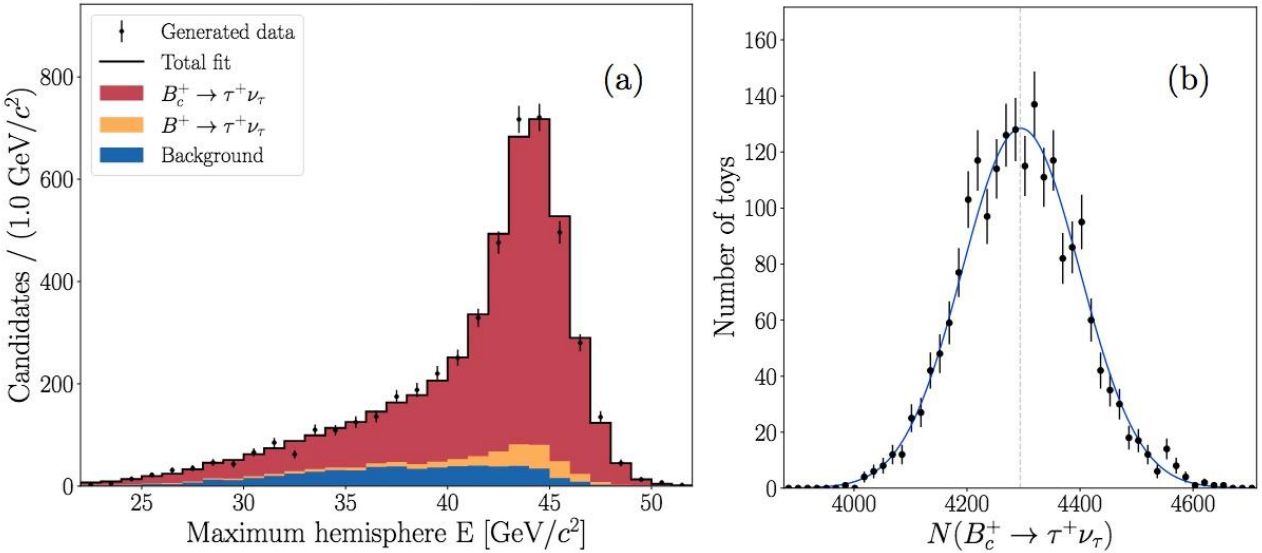

Figure 6: (a) Result of a single pseudoexperiment fit, where the peaking signal is clearly distinguishable from the background. (b) Signal yields measured in 2000 pseudoexperiment fits, where the generated value is indicated by the dashed vertical line.

Bc->Tau nu Yields

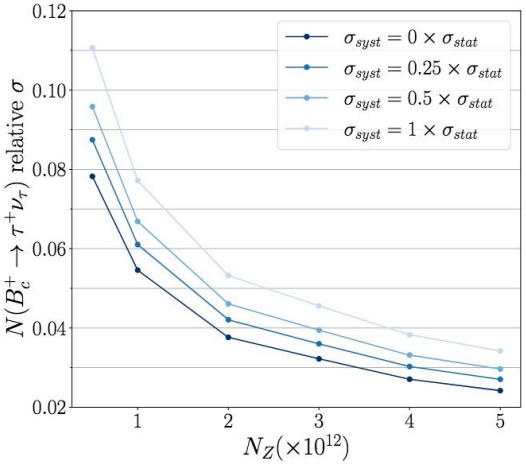

Figure 7: Relative precision on the signal yield as a function of N_Z. The signal yields at each N_Z value are taken from the cut optimisation procedure, and the statistical uncertainties are measured in pseudoexperiment fits. Different levels of systematic uncertainty relative to the statistical uncertainty are also shown.

$N_Z(\times 10^{12})$	$N(B_c^+ \to \tau^+\nu_\tau)$	Relative σ (%)
0.5	430 ± 33	7.8
1	858 ± 46	5.5
2	1717 ± 64	3.8
3	2578 ± 83	3.2
4	3436 ± 93	2.7
5	4295 ± 103	2.4

Table 1: Estimated signal yields as a function of N_Z, where the uncertainties quoted are statistical only. The yield central values are determined from the cut optimisation procedure, and the uncertainties from pseudoexperiment fits.

Towards Branching Fraction

With $B_c^+ \to J/\psi\mu^+\nu_\mu$ as a normalisation mode, the ratio of branching fractions

$$R_c = \frac{\mathcal{B}(B_c^+ \to \tau^+\nu_\tau)}{\mathcal{B}(B_c^+ \to J/\psi\mu^+\nu_\mu)} = \frac{N(B_c^+ \to \tau^+\nu_\tau)}{N(B_c^+ \to J/\psi\mu^+\nu_\mu)} \times \frac{\epsilon(B_c^+ \to J/\psi\mu^+\nu_\mu)}{\epsilon(B_c^+ \to \tau^+\nu_\tau)} \times \frac{\mathcal{B}(J/\psi \to \mu^+\mu^-)}{\mathcal{B}(\tau^+ \to \pi^+\pi^+\pi^-\bar{\nu}_\tau)}$$

It is also possible to determine an absolute branching fraction for the signal decay,

$$\mathcal{B}(B_c^+ \to \tau^+\nu_\tau) = R_c \times \mathcal{B}(B_c^+ \to J/\psi\mu^+\nu_\mu)^{\mathrm{SM}},$$

Results

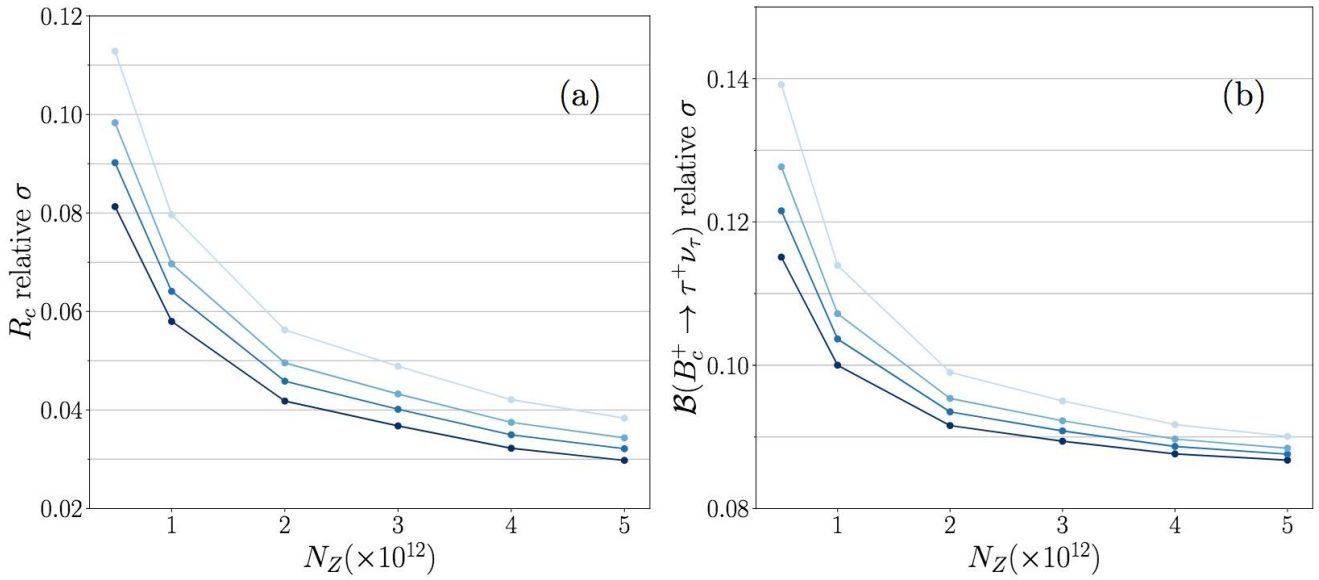

Figure 8: (a) Relative precision on the ratio of branching fractions $R = \mathcal{B}(B_c^+ \to \tau^+\nu_\tau)/\mathcal{B}(B_c^+ \to J/\psi\mu^+\nu_\mu)$ as a function of N_Z. (b) Relative precision on $\mathcal{B}(B_c^+ \to \tau^+\nu_\tau)$ as a function of N_Z, using a SM prediction for $\mathcal{B}(B_c^+ \to J/\psi\mu^+\nu_\mu)$. The different shades of blue correspond to different levels of systematic uncertainty on $N(B_c^+ \to \tau^+\nu_\tau)$ relative to the statistical uncertainty, following the same colour scheme as Fig. 7.

New physics - 2HDM

Thanks to Olcyr Sumensari for the interpretation work, which is based on the analysis precision estimates

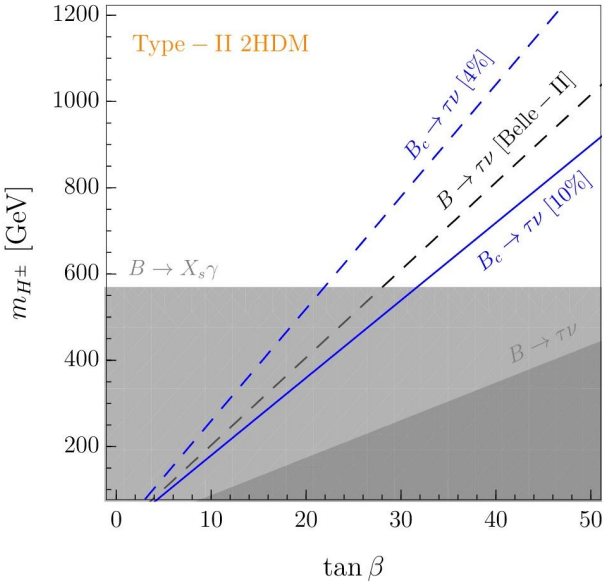

Figure 9: Expected constraints on the plane $\tan\beta$ vs. $m_{H^\pm}$ for type-II 2HDM derived by assuming a relative uncertainty on $\Gamma(B_c^+ \to \tau^+\nu_\tau)/|V_{cb}|^2$ of 10% (solid blue line) and 4% (dashed blue line). Current constraints obtained from $\mathcal{B}(B \to X_s\gamma)$ [64] and $\mathcal{B}(B^+ \to \tau^+\nu_\tau)$ [61] are depicted by the grey regions. Prospects for a $\mathcal{B}(B^+ \to \tau^+\nu_\tau)$ measurement at Belle-II are depicted by the grey dashed line, obtained under the assumption of 5% uncertainty on the branching fraction [69].

New physics - Leptoquarks

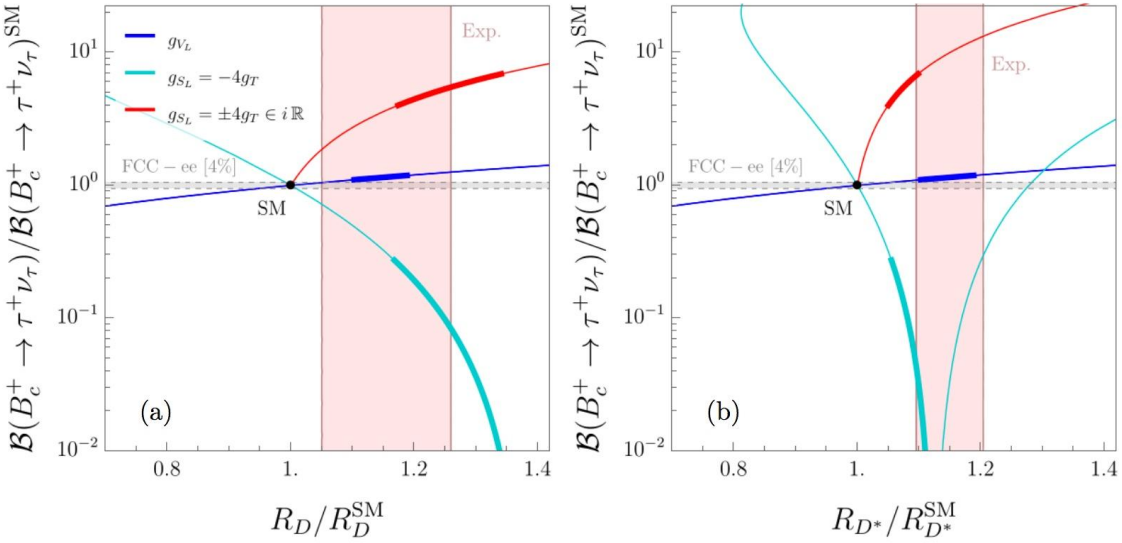

Figure 10: Predictions for (a) $R_D/R_D^{\rm SM}$ and (b) $R_{D^*}/R_{D^*}^{\rm SM}$ are plotted against the ratio $\mathcal{B}(B_c^+ \to \tau^+\nu_\tau)/\mathcal{B}(B_c^+ \to \tau^+\nu_\tau)^{\rm SM}$ in several effective scenarios: (i) g_{V_L} (blue), (ii) $g_{S_L} = -4g_T$ (cyan), and (iii) $g_{S_L} = +4g_T \in i\,\mathbb{R}$ (red), which are defined at $\Lambda \approx 1$ TeV. The thick lines correspond to the values of the effective couplings favoured by the current fit to $b \to c\tau\nu_\tau$ data [71]. The red shaded regions denote the current experimental averages of R_D and R_{D^*} at 1σ accuracy [23]. The grey region corresponds to the estimated sensitivity of 4% precision on $\Gamma(B_c^+\tau^+\nu_\tau)/|V_{cb}|^2$ at FCC-ee.

Summary

The sensitivities for both the branching fraction of $B_c^+ \to \tau^+\nu_\tau$ and the ratio $R_c = \mathcal{B}(B_c^+ \to \tau^+\nu_\tau)/\mathcal{B}(B_c^+ \to J/\psi\mu^+\nu_\mu)$ are estimated as a function of the number of collected Z decays, where a relative precision of around 4% is achieved for R_c with $N_Z = 5 \times 10^{12}$. The precision on the absolute branching fraction is limited to around 8% due to knowledge of the $B_c^+ \to J/\psi\mu^+\nu_\mu$ decay form factors, which can be improved through dedicated measurements of this mode in future.

The impact of a measurement of $B_c^+ \to \tau^+\nu_\tau$ on NP scenarios is also discussed. In particular, it is shown that such a measurement at FCC-ee can constrain a large region of the $(\tan\beta, m_{H^\pm})$ plane in the type-II 2HDM, which cannot be covered by other flavour-physics measurements. Recently, leptoquark models have received significant attention as the only viable explanation of the B-physics anomalies in both charged and neutral current processes. A precise measurement of the branching fraction of $B_c^+ \to \tau^+\nu_\tau$ at FCC-ee could fully probe the interpretations of R_D and R_{D^*} that are permitted under existing constraints.

In summary, this work demonstrates why FCC-ee is the most well-suited environment for a measurement of the branching fraction of the $B_c^+ \to \tau^+\nu_\tau$ decay, and represents the first FCC-ee analysis to use common software tools from EDM4HEP through to final analysis.

The context

Analysis history

- September 2020
  - Met Donal Hill (LHCb) who was attending a snowmass tutorial
  - Wished to publish a result by end summer 2021
- November 2020
  - First presentation at the 4th FCC Physics and Experiment WS
- January 2021
  - Yasmine expressed interest and presented plans at FCC France
- Mars 2021
  - Olcyr joined, dream team completed
- May 2021
  - pre-print on arxiv
- June 2021
  - submit to JHEP
  - start with Bc->J/Psi mu nu (leading uncertainty)